nature communications

Article

https://doi.org/10.1038/s41467-025-59364-3

Iron-catalyzed sequential hydrosilylation

Received: 30 January 2025

Accepted: 17 April 2025

Published online: 09 May 2025

Check for updates

Xue Wang[1,3], Jiajin Zhao[1,3], Dongyang Wang[2], Liang Deng[2] & Zhan Lu[1]

Highly regio-, diastereo- and enantioselective iron-catalyzed sequential hydrosilylation of *o*-alk-*n*-enyl-phenyl silanes with alkynes is reported for various 5-, 6-, and 7-membered benzosilacycles in 60-94% yields with up to 95:5 *rr*, 95:5 *dr*, and 99% *ee*. Chiral fully carbon-substituted silicon-stereogenic benzosilacycles could also be obtained via triple hydrosilylation reactions. The unique electronic effect of ligands is observed while adjusting the regioselectivity and enantioselectivity in hydrosilylation reactions. A possible mechanism has been proposed by variable time normalization analysis (VTNA) and H/D exchange experiment.

Silasubstitution strategy was regarded as an innovative strategy to develop new materials and pesticides, and has found interesting applications in many fields (Fig. 1A)[1–16]. A series of 5-, 6-, and 7-membered benzosilacycles had been constructed using transition metal catalysis, such as Rh[17–29], Pd[30–37], Ru[38], Ir[39], Sc[40], and Ni[41] etc. (Fig. 1B). It should be noted that neither the catalytic cyclization for the synthesis of benzosilacycles containing two Si-H bonds which could be further derivatized, nor the construction of vicinal chiral carbon and silicon-centers in benzosilacycles has been reported. Although intramolecular hydrosilylation of alkenes containing mono-substituted silanes could be proposed to deliver the benzosilacycles containing two Si–H bonds which could undergo further sequential reactions[42], there were several challenges: (1) The side reactions, such as hydrogenation, intermolecular hydrosilylation, and over functionalization of Si–H bonds, could significantly affect the production of benzosilacycles containing two Si–H bonds. (2) Compared to the C–C bond, the transition state was more flexible due to the longer C–Si bond which prompted more hardship in differentiating two enantiotopic faces. (3) For the sequential reactions, the difficulty to achieve the compatibility and control the sequence was increased in the presence of the multiple active Si–H bond and similar unsaturated C–C bonds in one pot. Additionally, although iron was the most earth-abundant transition metal[43], neither the iron-catalyzed hydrosilylation for the construction of benzosilacycles nor sequential hydrofunctionalization have been reported until now. Here, we reported an iron-catalyzed sequential hydrosilylation of n-alkenyl-phenyl silanes with alkynes to afford 5-, 6-, and 7- membered various benzosilacycles in good yields with excellent diastereo- and enantioselectivitiy, and sequential reactions in one pot for the construction of fully carbon-substituted silicon center, as shown in Fig. 1C. In this process, while changing the electronic effects on ligands, the regioselectivity and enantioselectivity of hydrosilylation reactions could be controlled.

Results: the iron-catalyzed sequential hydrosilylation to construct benzosilacycles

Results 1: the construction of 5- and 6-membered various benzosilacycles benzosilacycles

At the beginning of the screening, simple (2-vinylphenyl)silane (**1a**) and 1,2-diphenylethyne (**2a**) were chosen as model substrates. Lithium tert-butoxide and toluene were used as a mild activator and solvent, respectively. The reaction using bidentate bipyridine iron dichloride complex did not provide hydrosilylation products (entry 1, Table 1). The PDI ligand promoted the intramolecular hydrosilylation to afford **3a′** in 35% yield without sequential hydrosilylation product **3a** (entry 2). Both Pybox and OIP ligands could promote the sequential reaction to deliver **3a** in 44% and 54% yield, respectively. Increasing the steric hindrance on oxazoline and imine could improve the reactivity (entries 5 and 6). The reaction using 1.2 equiv of **1a** afforded **3a** in 96% yield (entry 7). Finally, the standard conditions were identified as using silane **1a** (1.2 equiv), 1,2-diphenylethyne **2a** (0.5 mmol), **Fe-3** (5 mol%), and LiO*t*Bu (15 mol%) in a solution of toluene (0.5 M) stirring at room temperature for 24 h. It should be noted that the catalyst **Fe-3** could distinguish the intermolecular hydrosilylation and intramolecular hydrosilylation, and also raise the activity of the reactions. More details are shown in supplementary information (Table S2)

Under the optimized conditions, the substrate scope was explored in Fig. 2A. Reactions of various diaryl alkynes containing ethers, halogens, heterocycles, diheteroaryl and dialkyl alkynes efficiently proceeded to afford desired *anti*-Markovnikov products **3a**–**3o** in 68-93% yields. The 5-methyl and 4-chloro group on aryl silane could

[1]Center of Chemistry for Frontier Technologies, Department of Chemistry, Zhejiang University, Hangzhou, China. [2]The State Key Laboratory of Organometallic Chemistry, Shanghai Institute of Organic Chemistry, Chinese Academy of Sciences, Shanghai, China. [3]These authors contributed equally: Xue Wang, Jiajin Zhao. e-mail: luzhan@zju.edu.cn

https://doi.org/10.1038/s41467-025-59364-3

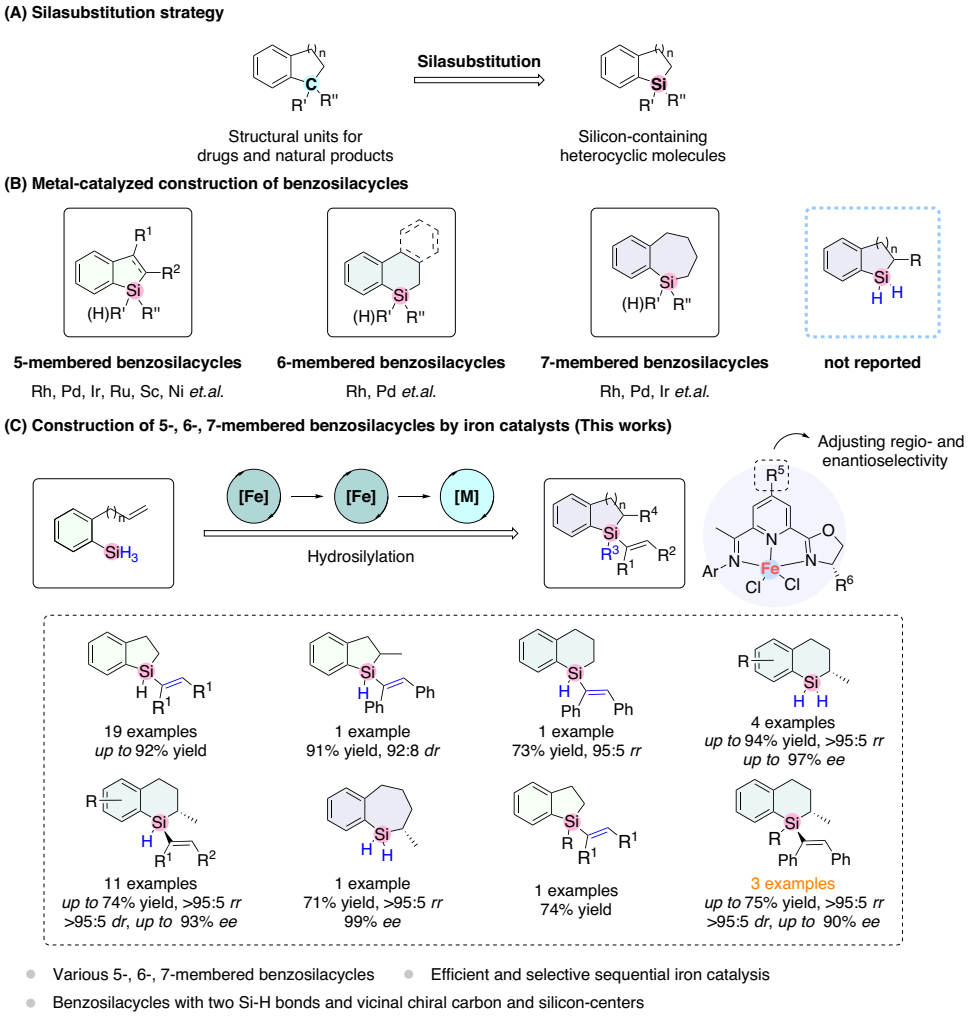

Fig. 1 | Benzosilacycles and their synthesis. A Silasubstitution strategy, **B** Metal-catalyzed construction of benzosilacycles, **C** This work: Construction of 5-, 6-, 7-membered benzosilacycles by iron catalysts. The green colour is about the construction of 5-membered benzosilacycles, blue colour is aboult the construction of 6-membered benzosilacycles and purple colour is about the construction of 7-membered benzosilacycles. The pink colour is about "Si".

be tolerated to access **3q** and **3r** in 85 and 81% yield, respectively. Time course is shown in supplementary information (SI Figs. 1 and 2)

As shown in supporting information Table S4, the reaction using **Fe-7** and Li*O*t*Bu in a solution of toluene at room temperature for 24 h afforded the mixed product in 78% yield with 50:50 *rr*. While using **Fe-16** with minor hindrance of oxazoline, only 22% yield and 50:50 *rr* are provided. While adjusting the steric hindrance of imine could realize the control of Markovnikov selectivity to deliver the 5-membered benzosilacycle **5a** in 91% yield with >95:5 *rr* and 92:8 *dr*. Then the use of **Fe-17** which was modified with the electronic donating group could increase the *anti*-Markovnikov regioselectivity to 15:85. The use of more sterically hindered on oxazoline **Fe-5** could improve the regioselectivity to afford 6-membered benzosilacycle **6a** in 75% yield with 95:5 *rr* (Fig. 2B).

Results 2: The construction of 6- and 7-membered various benzosilacycles benzosilacycles

When (2-(but-3-en-1-yl)phenyl)silane (**7a**) was used as a substrate, the asymmetric iron-catalyzed intramolecular hydrosilylation could occur smoothly to deliver 6-membered dihydro-benzosilacycle **8a**. As shown in Table 2, the use of **Fe-8** afford the product with 79% *ee*. While electronic donating group was added to the ligand, 90% *ee* was provided. Electronic effects on the ligand might have a positive impact on enantioselectivity of intramolecular hydrosilylation reactions. The reactions of substrates with 4-methory, 3-fluoro, and 4-TBSO- groups were pushed on smoothly to afford products **8b**–**8d** in 87–90% yields with 93:7 to >95:5 *rr*, and 90–97% *ee* (Fig. 3A). The absolute configuration was consistent with that previously reported by our group[43].

After the first intramolecular hydrosilylation completed, the complex **Fe-3** (5 mol%), Li*O*t*Bu (15 mol%), alkynes (1 eq.) and toluene (0.5 M) were added in the system. The sequential reactions could be carried out to provide the 6-membered monohydro-benzosilacycle **10a** with vicinal chiral carbon and silicon centers in 65% yield with >95:5 *rr*, >95:5 *dr*, and 93% *ee* (Fig. 3B)[44,45]. The sequential reactions of substrates with 4-methory, 3-fluoro, and 4-TBSO- groups were carried out smoothly to afford **10b**–**e** in 60–70% yields with excellent regio-, diastereoselectivity (>95:5 *rr*, >95:5 *dr*), and 86-93% *ee*. The substrates with heterocycle and alkyl alkyne could also be pushed on efficiently. For the unsymmetrical alkyne but-1-yn-1-ylbenzene, sequential reaction afforded the *α*-syn-selective product **10j** in 75% yield. The complex molecular empagliflozin ntermediate was also easily transformed into the corresponding chiral silanes **10k** with uncompromised 80% yield with 93% *ee*. The absolute configuration of the resulting carbon and silicon-stereogenic center in **10l** was unambiguously determined by an X-ray diffraction. Excitedly, 7-membered carbon-stereogenic benzosilacycle **12a** could also be constructed in 73% yield with 99% *ee* while using (2-(pent-4-en-1-yl)phenyl)silane (**11a**) in the presence of iron catalyst (Fig. 3C).

https://doi.org/10.1038/s41467-025-59364-3

Table 1 | Optimizations for sequential hydrosilylation

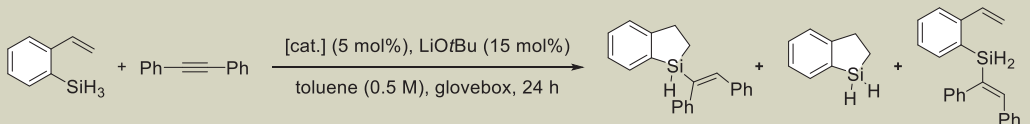

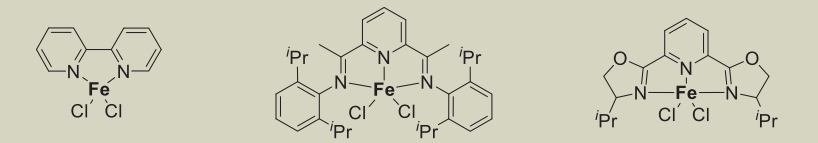

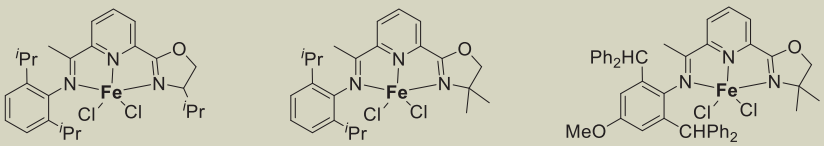

Entry	Catalyst	Yield of 3a (%)[a]	Yield of 3a′ (%)	Yield of 3a″ (%)
1	**L1-Fe**	–	–	–
2	**L2-Fe**	–	35	–
3	**L3-Fe**	44	–	3
4	**Fe-1**	53	–	–
5	**Fe-2**	79	–	–
6	**Fe-3**	84	–	–
7[b]	**Fe-3**	96 (90)[c]	–	–

[a]Reaction conditions: **1a** (0.5 mmol), **2a** (0.5 mmol), **cat**. (0.025 mmol), LiO*t*Bu (0.075 mmol), toluene (1 mL).
[b]Using 1.2 equiv. of **1a**.
[c]Isolated yield in the parentheses.

The reaction of **1a** with **2a** could be carried out in a gram scale to afford **3a** with 1.28 g in 82% yield (Fig. 4A, **eq.1**). The reaction of **7a** could be performed on gram scale, providing 6-membered benzosilacycles **10a** with 1.06 g in 62% yield (Fig. 4A, **eq.2**). Treatment of **3a** with 1-ethynyl-4-methoxybenzene in the presence of a dicobalt carbonyl N-heterocyclic carbene [(IPr) $Co_2(CO)_7$] (IPr = 1,3-*di*(2,6-diisopropylphenyl)imidazol-2-ylidene) complex provided 5-membered heterocycles derivatives **14a** in 74% yield (Fig. 4B **eq.3**)[46–49]. Terminal alkene, terminal alkyne and α, β unsaturated ketone could be used as partners to convert to fully carbon-substituted silicon-stereogenic heterocycles derivatives (**15a, 16a** and **17a**) in the presence of Karstedt's catalyst (Fig. 4B**, eq.4**–**6**)[50–52]. It is interesting that three stereocenters benzosilacycles **17a** could be obtained, which was quite difficult to be afforded by using other methods.

Deuterium-labeling experiments were conducted to explore the mechanism in those asymmetric hydrosilylation processes as shown in Fig. 5. The silicon-deuterated product **19a**-d_3 or **21a**-d_3 was afforded by the asymmetric sequence hydrosilylation of unsaturated C-C bonds with silane-d_3 (**18a** or **20a**) catalyzed by iron catalyst. The result suggested that insertion was regioselective and irreversible (**eq.7** and **eq.8**)[53]. The fact that the product **21a′** with deuterium incorporation into the α-carbon was not generated indicated the impossibility of a Fe-H or Fe-D intermediate in the catalytic cycle, because facile H/D exchange between C_α–H and Fe–D would otherwise occur through reversible olefin insertion into the Fe-D bond[54,55]. When intramolecular hydrosilylation with a 1:1 mixture of silane-d_3 (**20a**) and silane **7b** was carried out and followed by the intermolecular hydrosilylation, silicon-deuterated products **21a** and **21b** were obtained (in *Supporting Information*). The construction of silicon-deuterated product **21b** and the next deuterium-labeling experiment in **eq.9**, giving **24a**-d_2 and **25a**-d_2, indicated that Si-Fe species might participate in the catalytic cycle.

Mechanistic interrogation was realized through kinetic studies using variable time normalization analysis (VTNA)[56–62]. VTNA was used to determined the reagent orders of the reaction components, from which we hypothesized the turnover-limiting step. This method was used to determined the kinetic order of the reaction components in the second step. Two different slopes were observed in Fig. 6a, where the kinetic profile of the reaction with two different iron catalyst concentrations was shown. When a first-order factor of catalyst concentration (t $[Fe]^1$) was used (Fig. 6c), two reaction progress curves failed to overlap. While using a 0.5-order correlation (t $[Fe]^{0.5}$), two reaction progress curves overlapped (Fig. 6b), indicating that the kinetic order for iron is a 0.5-order rather than the first order. It was speculated that the active intermediates of iron catalyst might exist in the form of dimers[63]. It also meant that the rate of reaction was relatively insensitive to changes in the concentration of the reactants, but not completely unaffected. Next, a superior reaction was observed when increasing substrate **8a** loading (Fig. 6d–f), corresponding to a first order. Same with substrate 8a, the result that a first order for substrate **2a** was obtained from VTNA (Fig. 6g–i). The observation of $[\mathbf{8a}]^1$ and $[\mathbf{2a}]^1$ suggested that one molecular **8a** and one molecular **2a** were involved in the turnover limiting step. More information were shown in (SI Figs. 3–5)

Based on the above mechanisms, the proposed mechanism was shown in Fig. 7. The Fe–Si species (**A**) was proposed through reducing **Fe-5** by $NaBHEt_3$ and silane[64–67]. Then alkene inserted in Fe–Si bond to generate iron alkyl species (**B**), which wonder go δ-bond metathesis with silane to regenerate species (**A**) and afford the hydrosilylation product (**8a**). The Fe–Si (**C**) obtained from (**8a**). Because the kinetic

https://doi.org/10.1038/s41467-025-59364-3

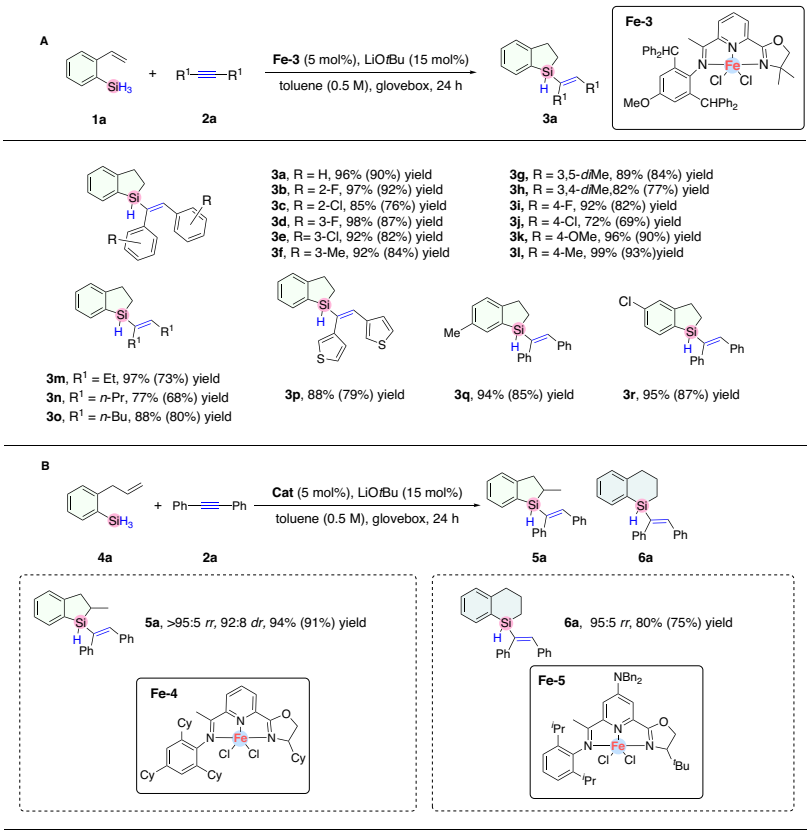

Fig. 2 | The scope of 2-vinylphenyl silanes and 2-allylphenyl silanes. [a]Standard conditions: **1a** (0.60 mmol), **2a** (0.50 mmol), cat. **Fe-3** (0.025 mol), LiO*t*Bu (0.075 mmol), toluene (1 mL). [b]Standard conditions: **4a** (0.3 mmol), **2a** (0.3 mmol), cat. **Fe-4** (0.015 mmol), LiO*t*Bu (0.045 mmol), toluene (0.6 mL). [c]Standard conditions: **4a** (0.30 mmol), **2a** (0.30 mmol), cat. **Fe-5** (0.015 mmol), LiO*t*Bu (0.045 mmol), toluene (0.6 mL). [d]Isolated yield in the parentheses. [e]Yields were determined by ^{1}H NMR using TMSPh as an internal standard. **A** The scope of 2-vinylphenyl silanes; **B** The scope of 2-allylphenyl silanes.

Table 2 | Optimizations for intramolecular hydrosilylation

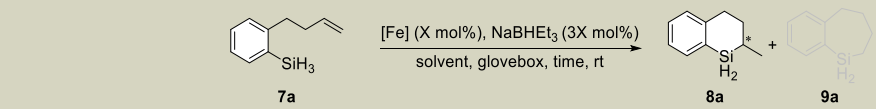

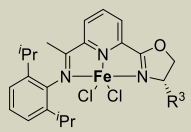

Fe-1 : R^3 = ^{i}Pr
Fe-6 : R^3 = Bn
Fe-7 : R^3 = Cy
Fe-8 : R^3 = ^{t}Bu

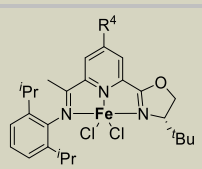

Fe-9 : R^4= NMe_2
Fe-5 : R^4= NBn_2

Entry	Catalyst	x	Base	Solvent	Time (h)	Yield[b] (%)	ee of 8a[c] (%)
1[a]	**Fe-1**	5	NaO*t*Bu	THF	12	60	58
2	**Fe-6**	5	NaO*t*Bu	THF	12	62	60
3	**Fe-7**	5	NaO*t*Bu	THF	12	66	61
4	**Fe-8**	5	NaO*t*Bu	THF	12	62 (83:17 *rr*)	75
5	**Fe-8**	5	$NaBHEt_3$	THF	12	90	74
6	**Fe-8**	5	$NaBHEt_3$	Neat	12	95	79
7	**Fe-5**	5	$NaBHEt_3$	Neat	12	73	90
8	**Fe-5**	2	$NaBHEt_3$	Neat	12	90	90
9	**Fe-5**	2	$NaBHEt_3$	Neat	3	91	91
10	**Fe-9**	2	$NaBHEt_3$	Neat	3	90	87

[a]Standard conditions: **7a** (0.50 mmol), cat. **Fe** (0.025 mol), NaO*t*Bu (0.075 mmol), THF (1 mL).
[b]Yields were determined by ^{1}H NMR using TMSPh as an internal standard.
[c]The enantiomeric excess ratio (*ee*) was determined by chiral HPLC.

https://doi.org/10.1038/s41467-025-59364-3

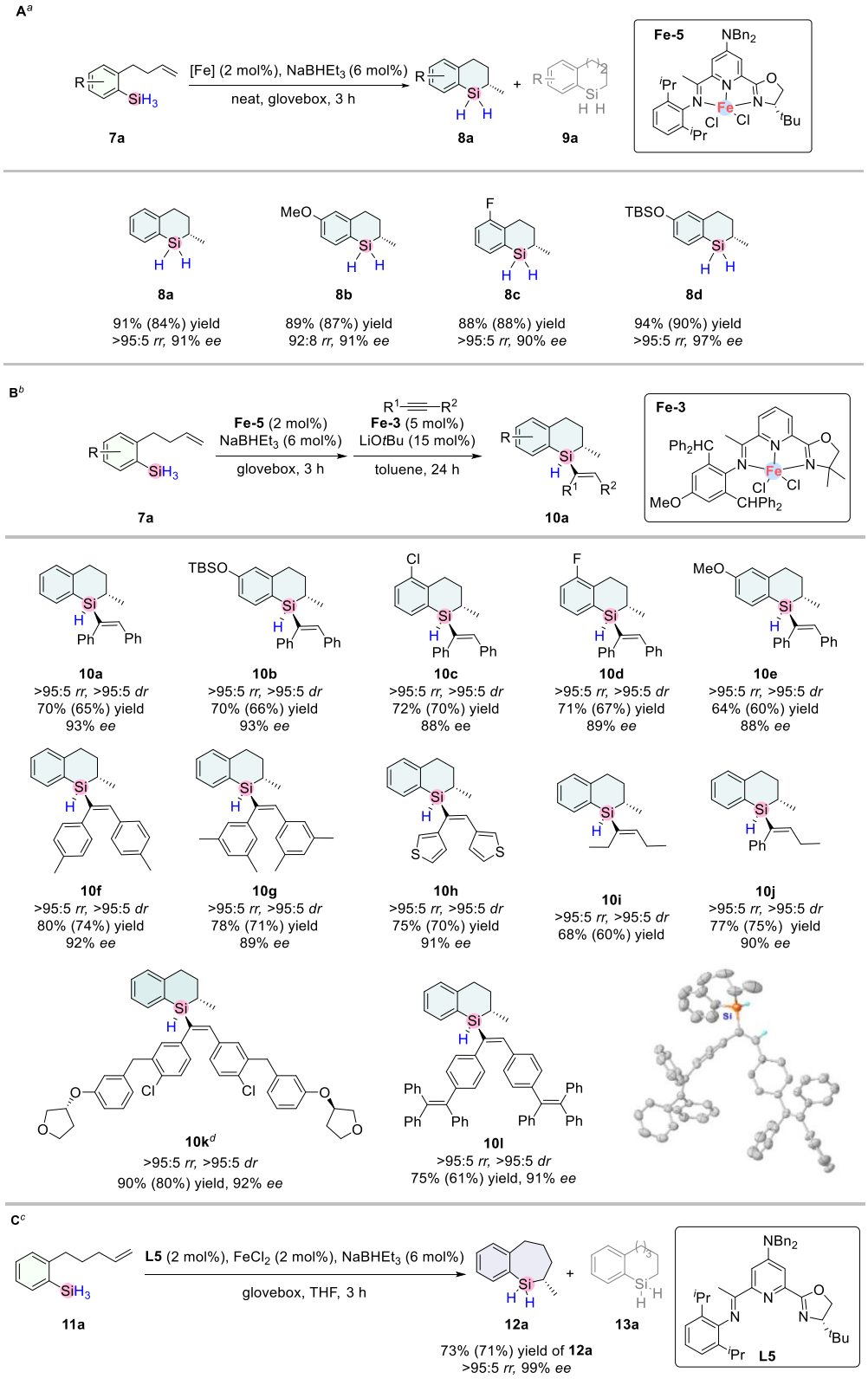

Fig. 3 | The scope of chiral benzosilacycles. [a]Standard conditions: **7a** (0.50 mmol), cat. **Fe-5** (0.010 mmol), $NaBHEt_3$ (0.030 mmol). [b]Standard conditions: **7a** (0.30 mmol), cat. **Fe-5** (0.006 mmol), $NaBHEt_3$ (0.018 mmol), cat. **Fe-3** (0.015 mmol), **2a** (0.30 mmol), LiO*t*Bu (0.045 mmol), toluene (0.6 mL). [c]Standard conditions: **11a** (0.30 mmol), L (0.006 mmol), $NaBHEt_3$ (0.018 mmol), THF (0.6 mL). [d]Standard conditions: **7a** (0.36 mmol). [e]Yields were determined by ^1H NMR using TMSPh as an internal standard. [f]Isolated yield in the parentheses. **A** The scope of benzosilacycles with two Si–H bonds; **B** The scope of benzosilacycles with vicinal chiral carbon and silicon-centers; **C** The scope of 7-membered benzosilacycles.

https://doi.org/10.1038/s41467-025-59364-3

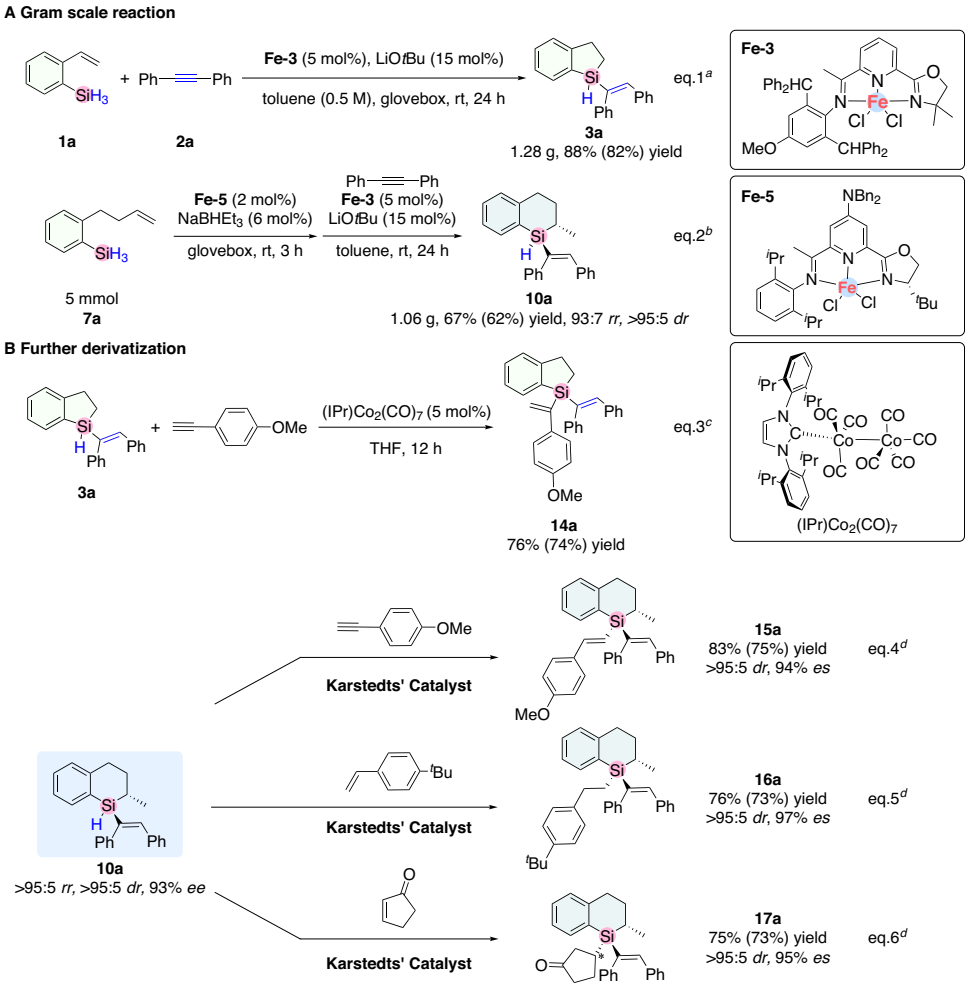

Fig. 4 | Gram scale reaction and further derivatization. [a]**eq.1** Gram scale reaction of **1a**, [b]**eq.2** Gram scale reaction of **7a**, [c]**eq.3** further derivatization of **3a**, [d]**eq.4-6** further derivatization of **10a**. **A**. Gram scale reaction of **1a** and **7a**. **B** further derivatization of **3a** and **10a**.

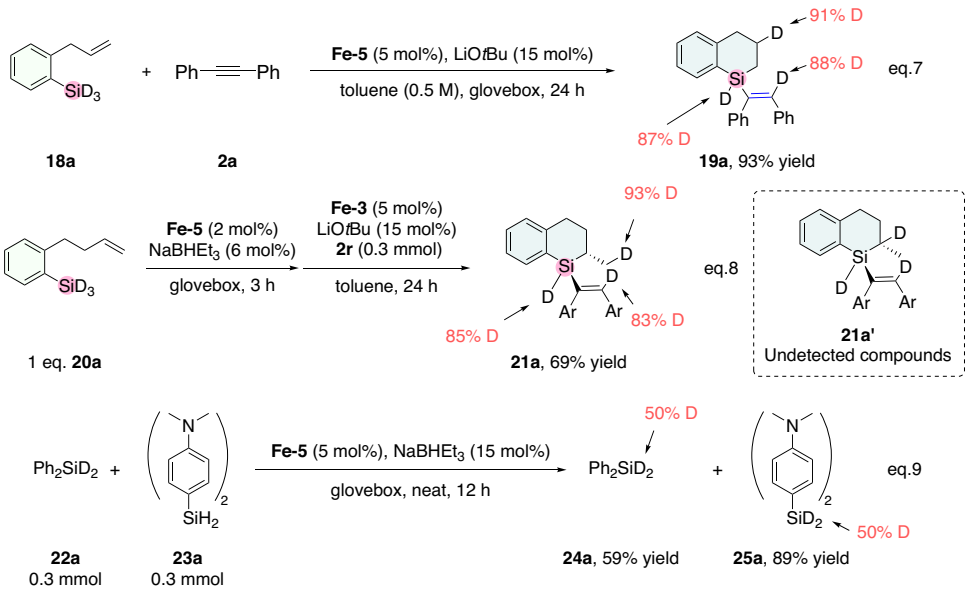

Fig. 5 | Mechanistic experiments to explore the active intermediate. eq.7-8 Deuterium-labeling experiments.

https://doi.org/10.1038/s41467-025-59364-3

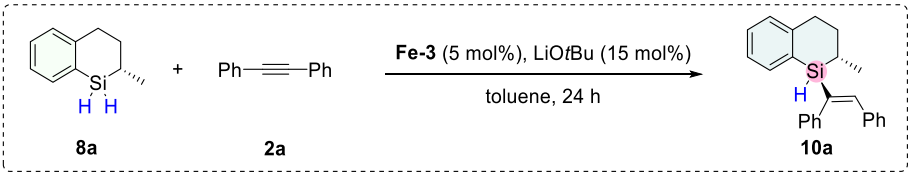

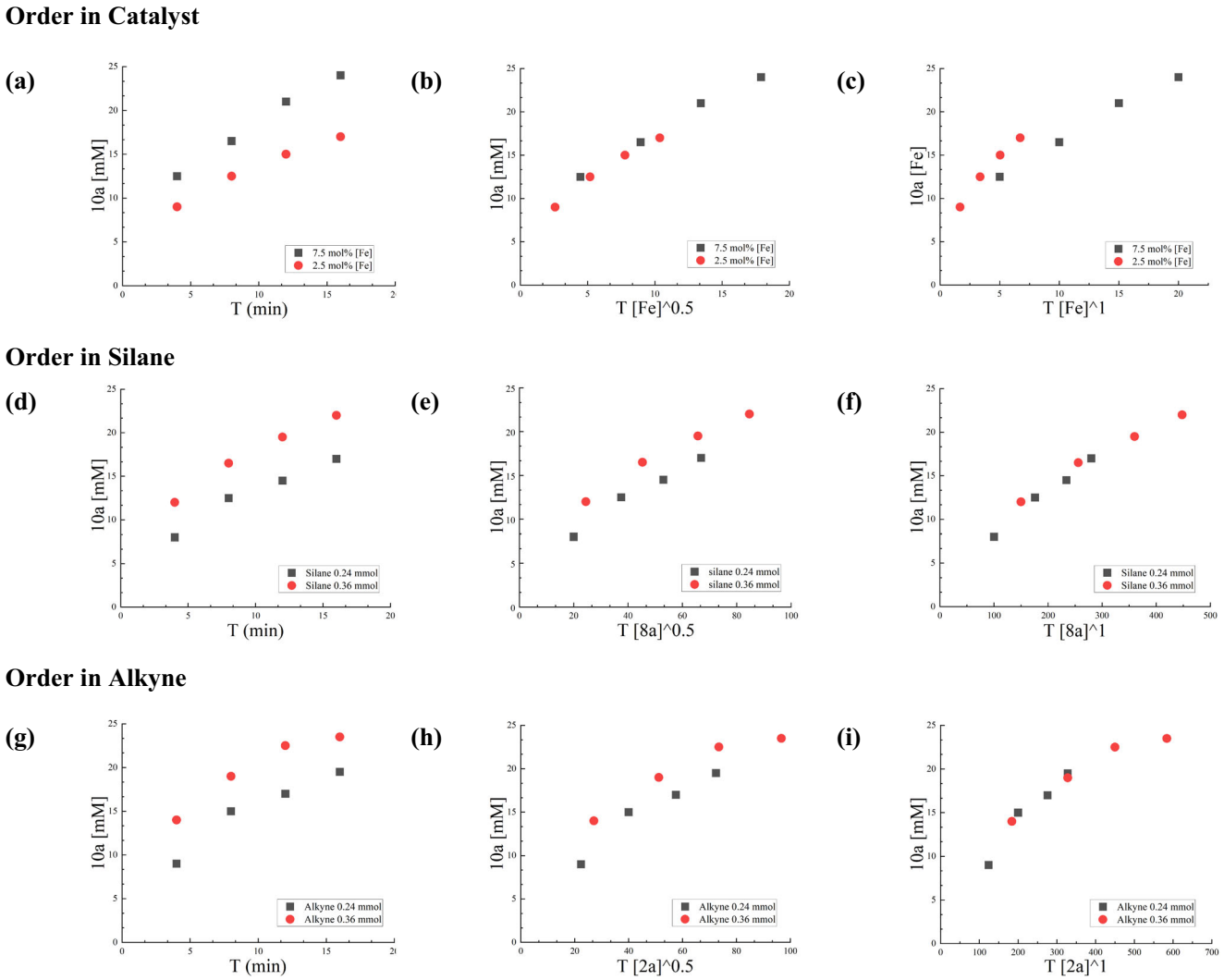

Fig. 6 | variable time normalization analysis. a–c VTNA analysis of catalyst, **d-f** VTNA analysis of silane, **g–i** VTNA analysis of alkyne.

order for iron is a 0.5-order rather than the first order, the active intermediates Fe–Si (**C**) might exist in the form of dimers, which was proposed and this proposal would be tested in our future work. Then alkyne inserted into Fe–Si bond to generate iron alkenyl species (**D**), which reacted with silane to regenerate Fe–Si species (**C**) and afforded the final product (**10a**). More studies were continuously under-going in our laboratory to gain an accurate understanding of the mechanism. The mechanism of Fe(0) species cannot be completely ruled out.

The primary models to predict the regiochemical outcome about the construction of 5- and 6-membered benzosilacycle were shown in Fig. 8. The primary models **PM**(**A**) and (**B**) provided similar possibility of Markovnikov and *anti*-Markovnikov hydrosilylation products **5a** and **6a**. While increasing the steric hindrance of imine, the primary models **PM**(**C**) was disfavored. While electronic donating groups added to ligand, electronegativity on Fe turned over. Then the primary models **PM**(**E**) become the dominant conformation and *anti*-Markovnikov product was provided. In the primary models, electronic donating groups on the ligand may exist in a resonant form, resulting in the electronegativity of Fe turning over. This resonant form might alter the size of ligand cavity, thus making the transition state more compact and improving the enantioselectivity of the reaction Fig. 8. More information were shown in (SI Figs. 6 and 7).

Discussion

In this work, we developed a mild iron-catalyzed system for the construction of 5-, 6-, and 7-membered benzosilacycles with highly regio-, diastereo- and seteroselectivity. Eight kinds of benzosilacycles including silacycles with vicinal chiral carbon and silicon-centers were successfully synthesized. The regioselectivity of hydrosilylation reactions could be controlled by iron catalyst step by step, and the kinetic order of the reaction components in the second step was determined by using variable time normalization analysis (VTNA). The development of more asymmetric iron-catalyzed reactions is ongoing in our laboratory.

https://doi.org/10.1038/s41467-025-59364-3

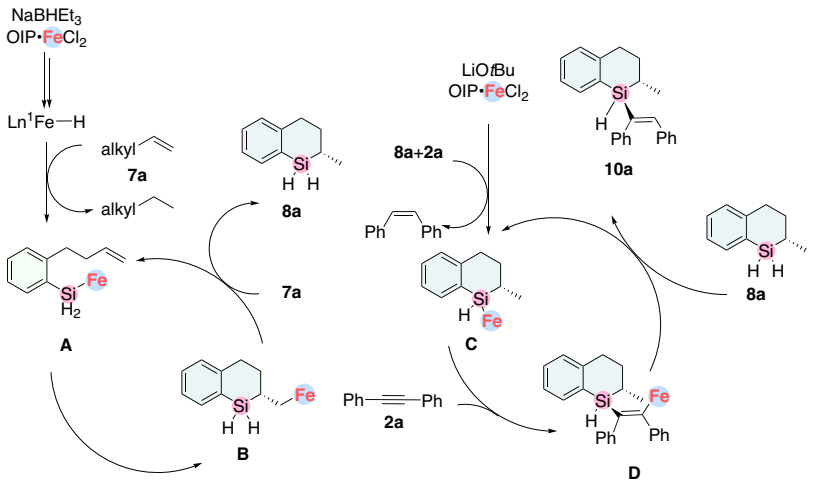

Fig. 7 | The proposed mechanism in sequential hydrosilylation. The proposed mechanism starts from intramolecular hydrosilylation, followed by intermolecular hydrosilylation.

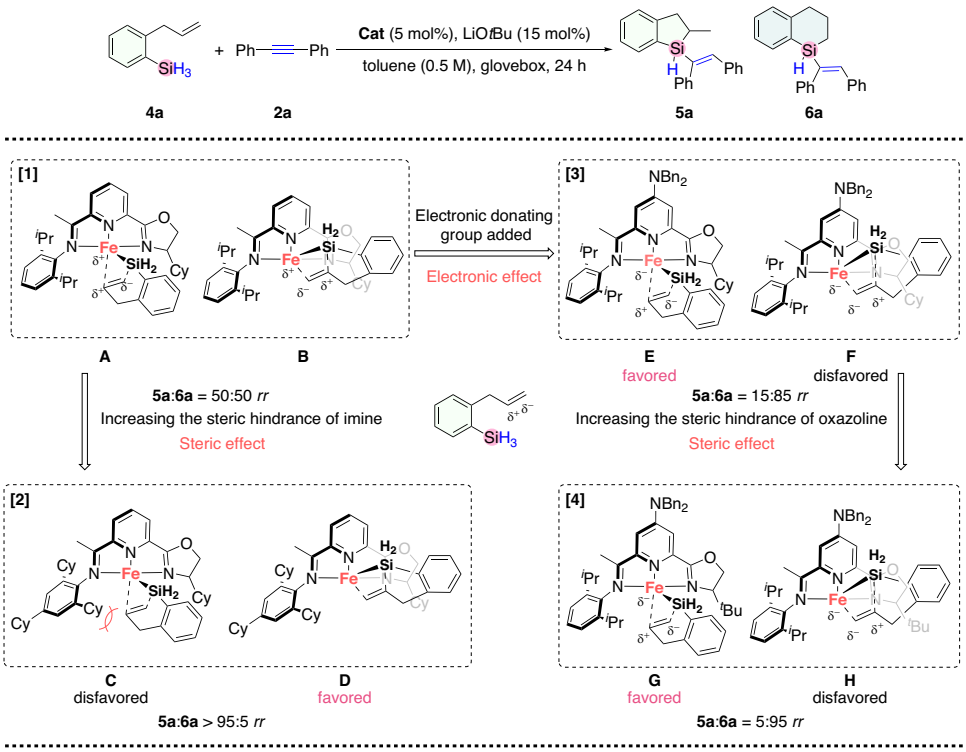

Fig. 8 | The primary models to predict the regiochemical outcome[a]. A–H The primary models to predict the regiochemical outcome to explain the selectivity in the construction of 5- and 6-membered benzosilacycles.

Methods

A 25 mL Schlenk flask equipped with a magnetic stirrer and a flanging rubber plug is dried with flame. When cooled to ambient temperature, it is transferred into glove box. Then **Fe-3** complex (0.025 mmol, 5 mol %), LiO*t*Bu (0.075 mmol, 15 mol%), **1a** (0.6 mmol, 1.2 equiv), alkynes (0.5 mmol), toluene (1 mL, 0.5 M) are added sequentially. The mixture is stirred at room temperature for 24 h. Then the resulting solution is transferred into room and quenched with 10 mL of PE and filtered through a pad of silica gel, washed with PE/AcOEt (10/1) (or other suitable solvent) (5 × 10 mL). The combined filtrate is concentrated and the yield is monitored by ^{1}H NMR analysis using TMSPh as an internal standard. The resulting solution is purified by flash column chromatography to give the corresponding product.

Data availability

The authors declare that the data Supplementary the findings of this study are available within the paper and its Supplementary Information file. The X-ray crystallographic coordinates for the structure of compound **10l** reported in this study have been deposited at the Cambridge Crystallographic Data Centre (CCDC), under deposition number 2383336. These data can be obtained free of charge from https://www.ccdc.cam.ac.uk. The Cambridge Crystallographic Data Centre via The experimental procedures and characterization of all new compounds are provided in the Supplementary Information. Data supporting the findings of this manuscript are also available from the authors upon request.

References

1. Wang, D. & Chan, T.-H. Chiral organosilicon compounds in asymmetric synthesis. *Chem. Rev.* **92**, 995–1006 (1992).
2. Oestreich, M. Silicon-stereogenic silanes in asymmetric catalysis. *Synlett* **11**, 1629–1643 (2017).
3. Li, L., Lai, G.-Q., Jiang, J.-X. & Xu, L.-W. The recent synthesis and application of silicon-stereogenic silanes: A renewed and significant challenge in asymmetric synthesis. *Chem. Soc. Rev.* **40**, 1777–1790 (2011).
4. Zhao, W.-T., Gao, F. & Zhao, D.-B. Recent progress in σ-bond cross-exchange reactions to access diverse silacycles. *Synlett* **29**, 2595–2600 (2018).
5. Ye, F. & Xu, L.-W. A glimpse and perspective of current organosilicon chemistry from the view of hydrosilylation and synthesis of silicon-stereogenic silanes. *Synlett* **32**, 1281–1288 (2021).
6. Wu, Y.-C. & Wang, P. Silicon-stereogenic monohydrosilane: synthesis and applications. *Angew. Chem. Int. Ed.* **61**, e202205382 (2022).
7. Yuan, W. & He, C. Enantioselective C–H functionalization toward silicon-stereogenic silanes. *Synthesis* **54**, 1939–1950 (2022).
8. Ge, Y.-C., Huang, J. K. & He, C. Transition-metal-catalyzed enantioselective C–H silylation. *Chem. Catal.* **2**, 2898–2928 (2022).
9. Huang, W.-S., Wang, Q., Yang, H. & Xu, L.-W. State-of-the-art advances in enantioselective transition-metal-mediated reactions of silacyclobutanes. *Synthesis* **54**, 5400–5408 (2022).
10. Gao, J.-H. & He, C. Chem. Chiral silanols: strategies and tactics for their synthesis. *Eur. J.* **29**, e202203475 (2023).
11. Showell, G. A. & Mills, J. S. Chemistry challenges in lead optimization: silicon isosteres in drug discovery. *Drug Discov. Today* **8**, 551–556 (2003).
12. Gately, S. & West, R. Novel therapeutics with enhanced biological activity generated by the strategic introduction of silicon isosteres into known drug scaffolds. *Drug Dev. Res.* **68**, 156–163 (2007).
13. Franz, A. K. & Wilson, S. O. Organosilicon molecules with medicinal applications. *J. Med. Chem.* **56**, 388–405 (2013).
14. Rémond, E., Martin, C., Martinez, J. & Cavelier, F. Silicon-containing amino acids: synthetic aspects, conformational studies, and applications to bioactive peptides. *Chem. Rev.* **116**, 11654–11684 (2016).
15. Fujii, S. & Hashimoto, Y. Progress in the medicinal chemistry of silicon: C/Si exchange and beyond. *Future Med. Chem.* **9**, 485–505 (2017).
16. Ramesh, R. & Reddy, D. S. Quest for novel chemical entities through Incorporation of silicon in drug scaffolds. *J. Med. Chem.* **61**, 3779–3798 (2018).
17. Onoe, M. et al. Rhodium-catalyzed carbon–silicon bond activation for synthesis of benzosilole derivatives. *J. Am. Chem. Soc.* **134**, 19477–19488 (2012).
18. Kuninobu, Y., Nakahara, T., Takeshima, H. & Takai, K. Rhodium-catalyzed Intramolecular silylation of unactivated C(sp^3)–H Bonds. *Org. Lett.* **15**, 426–428 (2013).
19. Zhao, W.-T., Lu, Z.-Q., Zheng, H., Xue, X.-S. & Zhao, D.-B. Rhodium-catalyzed 2-arylphenol-derived six-membered silacyclization: straightforward access toward dibenzooxasilines and silicon-containing planar chiral metallocenes. *ACS Catal.* **8**, 7997 (2018).
20. Chang, X., Ma, P. L., Chen, H. C., Li, C. Y. & Wang, P. Asymmetric synthesis and application of chiral spirosilabiindanes. *Angew. Chem. Int. Ed.* **59**, 8937–8940 (2020).
21. Mu, D. et al. Streamlined construction of silicon-stereogenic silanes by tandem enantioselective C–H silylation/alkene hydrosilylation. *J. Am. Chem. Soc.* **142**, 13459–13468 (2020).
22. Tang, R.-H. et al. Catalytic asymmetric trans-selective hydrosilylation of bisalkynes to access AIE and CPL-active silicon-stereogenic benzosiloles. *iScience* **23**, 101268 (2020).
23. Yang, B., Yang, W., Guo, Y.-H., You, L.-J. & He, C. Enantioselective silylation of aliphatic C–H bonds for the synthesis of silicon-stereogenic dihydrobenzosiloles. *Angew. Chem. Int. Ed.* **59**, 22217–22222 (2020).
24. Chen, S. Y. et al. Enantioselective construction of six- and seven-membered triorgano-substituted silicon-stereogenic heterocycles. *Nat. Commun.* **12**, 1249–1258 (2021).
25. Guo, Y. H., Liu, M. M., Zhu, X. J., Zhu, L. R. & He, C. Catalytic asymmetric synthesis of silicon-stereogenic dihydrodibenzosilines: silicon central-to-axial chirality relay. *Angew. Chem. Int. Ed.* **60**, 13887–13891 (2021).
26. Yuan, W. et al. Asymmetric synthesis of silicon-stereogenic monohydrosilanes by dehydrogenative C–H silylation. *Org. Lett.* **23**, 1367–1372 (2021).
27. Huang, Y. H. et al. Enantioselective synthesis of silicon-stereogenic monohydrosilanes by rhodium-catalyzed intramolecular hydrosilylation. *Angew. Chem. Int. Ed.* **61**, e202113052 (2022).
28. Gou, F.-H., R, F., W, Y. C. & Wang, P. Catalytic kinetic resolution of monohydrosilanes via rhodium catalyzed enantioselective intramolecular hydrosilylation. *Angew. Chem. Int. Ed.* **63**, e202404732 (2024).
29. Zeng, Y. et al. Rhodium-catalyzed dynamic kinetic asymmetric hydrosilylation to access silicon-stereogenic center. *Angew. Chem. Int. Ed.* **61**, e202214147 (2022).
30. Meng, T. H., Ouyang, K. B. & Xi, Z. F. Palladium-catalyzed cleavage of the Me–Si bond in ortho-trimethylsilyl aryltriflates: synthesis of benzosilole derivatives from ortho-trimethylsilyl aryltriflates and alkynes. *RSC Adv.* **3**, 14273 (2013).
31. Zhao, W. T., Gao, F. & Zhao, D. B. Intermolecular σ-bond cross-exchange reaction between cyclopropenones and (benzo)silacyclobutanes: straightforward access towards sila(benzo)cycloheptenones. *Angew. Chem. Int. Ed.* **57**, 6329 (2018).
32. Qin, Y., Han, J. L., Ju, W. C. & Zhao, D. B. Ring Expansion to 6-, 7-, and 8-membered benzosilacycles through strain-release silicon based cross-coupling. *Angew. Chem. Int. Ed.* **59**, 8481–8485 (2020).
33. Qin, Y., Li, L. H., Liang, J.-Y., Li, K. L. & Zhao, D. B. Silacyclization through palladium-catalyzed intermolecular silicon-based C(sp^2)–C(sp^3) cross coupling. *Chem. Sci.* **12**, 14224–14229 (2021).
34. Wang, X. C., Wang, H. R., Xu, X. F. & Zhao, D. B. Ring expansion to 8-membered silacycles through formal cross-dimerization of 5-membered palladacycles with silacyclobutanes. *Eur. J. Org. Chem.* 2021, 3039–3042.
35. Shi, Y. F. et al. Sila-spirocyclization involving unstrained C(sp^3)–Si bond cleavage. *Nat. Commun.* **13**, 6697 (2022).
36. Yin, K.-L. et al. Enantioselective construction of sila-bicyclo[3.2.1] scaffolds bearing both carbon- and silicon-stereocenters. *ACS Catal.* **12**, 13999–14005 (2022).
37. Zhang, J. Y. et al. Reversing site-selectivity in formal cross-dimerization of benzocyclobutenones and silacyclobutanes. *CCS Chem.* **5**, 1753–1762 (2023).
38. Fang, H. Q., Hou, W. J., Liu, G. X. & Huang, Z. Ruthenium-catalyzed site-selective intramolecular silylation of primary C–H bonds for synthesis of sila-heterocycles. *J. Am. Chem. Soc.* **139**, 11601–11609 (2017).
39. Su, B. & Hartwig, J. F. Ir-catalyzed enantioselective, intramolecular silylation of methyl C–H bonds. *J. Am. Chem. Soc.* **139**, 12137–12140 (2017).
40. Zhan, G. et al. Enantioselective construction of silicon-stereogenic silanes by scandium-catalyzed intermolecular alkene hydrosilylation. *Angew. Chem. Int. Ed.* **57**, 12342–12346 (2018).
41. Zhang, J. Y., Yan, N., Ju, C. W. & Zhao, D. B. Nickel(0)-catalyzed asymmetric ring expansion toward enantioenriched silicon-

stereogenic benzosiloles. *Angew. Chem. Int. Ed.* **60**, 25723–25728 (2021).
42. Lu, W. X., Zhao, Y. M. & Meng, F. K. Cobalt-catalyzed sequential site- and stereoselective hydrosilylation of 1,3- and 1,4-enynes. *J. Am. Chem. Soc.* **144**, 5233–5240 (2022).
43. Cheng, B., Liu, W. B. & Lu, Z. Iron-catalyzed highly enantioselective hydrosilylation of unactivated terminal alkenes. *J. Am. Chem. Soc.* **140**, 5014–5017 (2018).
44. Lgawa, K., Yoshihiro, D., Ichikawa, N., Kokan, K. & Tmooka, K. Catalytic enantioselective synthesis of alkenylhydrosilanes. *Angew. Chem. Int. Ed.* **51**, 12745 (2012).
45. Wen, H. N., Wan, X. L. & Huang, Z. Asymmetric synthesis of silicon-stereogenic vinylhydrosilanes by cobalt-catalyzed regio- and enantioselective alkyne hydrosilylation with dihydrosilanes. *Angew. Chem. Int. Ed.* **57**, 6319 (2018).
46. Wang, D. Y. et al. Markovnikov hydrosilylation of alkynes with tertiary silanes catalyzed by dinuclear cobalt carbonyl complexes with NHC ligation. *J. Am. Chem. Soc.* **143**, 12847 (2021).
47. Gao, Y. F., Wang, L. J. & Deng, L. Distinct catalytic performance of cobalt(I)–N heterocyclic carbene complexes in promoting the reaction of alkene with diphenylsilane: selective 2,1-hydrosilylation, 1,2-hydrosilylation, and hydrogenation of alkene. *ACS Catal.* **8**, 9637–9646 (2018).
48. Liu, Y. & Deng, L. Mode of activation of cobalt(II) amides for catalytic hydrosilylation of alkenes with tertiary silanes. *J. Am. Chem. Soc.* **139**, 1798–1801 (2017).
49. Sun, J. & Deng, L. Cobalt complex-catalyzed hydrosilylation of alkenes and alkynes. *ACS Catal.* **6**, 290–300 (2016).
50. Downing, C. M. & Kung, H. H. Diethyl sulfide stabilization of platinum-complex catalysts for hydrosilylation of olefins. *Catal. Commun.* **12**, 1166–1169 (2011).
51. Sommer, L. H., Lyons, J. E. & Fujimoto, H. Stereochemistry of asymmetric silicon. XV. stereospecific hydrosilation and exchange reactions of $R_3Si^*H(D)$ Catalyzed by Group VIII Metal Centers. *J. Am. Chem. Soc.* **91**, 7051 (1969).
52. Book, A. G., Pannell, K. H. & Anderson, D. G. α-Silyl-*cis*-stilbenes from silylcarbonium ions and from the platinum-catalyzed addition of silanes to diphenylacetylene. *J. Am. Chem. Soc.* **90**, 4374 (1968).
53. Lu, P., Wang, H. L., Mao, Y. H., Hong, X. & Lu, Z. Cobalt-catalyzed enantioconvergent hydrogenation of minimally functionalized isomeric olefins. *J. Am. Chem. Soc.* **144**, 17359–17364 (2022).
54. Du, X. Y., Zhang, Y. L., Peng, D. J. & Huang, Z. Base–metal-catalyzed regiodivergent alkene hydrosilylations. *Angew. Chem. Int. Ed.* **55**, 6671–6675 (2016).
55. Hu, M. Y. et al. Iron-catalyzed regiodivergent alkyne hydrosilylation. *J. Am. Chem. Soc.* **142**, 16894–16902 (2020).
56. Choudhary, S., Cannas, D. M., Wheatley, M. & Larrosa, I. A manganese(I) tricarbonyl-catalyst for near room temperature alkene and alkyne hydroarylation. *Chem. Sci.* **13**, 13225–13230 (2022).
57. Burés, J. A simple graphical method to determine the order in catalyst. *Angew. Chem. Int. Ed.* **55**, 2028–2031 (2016).
58. Burés, J. Variable time normalization analysis: general graphical elucidation of reaction orders from concentration profiles. *Angew. Chem. Int. Ed.* **55**, 16084–16087 (2016).
59. Blackmond, D. G. Kinetic profiling of catalytic organic reactions as a mechanistic tool. *J. Am. Chem. Soc.* **137**, 10852–10866 (2015).
60. Baxter, R. D., Sale, D., Engle, K. M., Yu, J. Q. & Blackmond, D. G. Mechanistic rationalization of unusual kinetics in Pd-catalyzed C–H olefination. *J. Am. Chem. Soc.* **134**, 4600–4606 (2012).
61. Lin, Z. P., Oliveira, J. C. A., Scheremetjew, A. & Ackermann, L. Palladium-catalyzed electrooxidative double C–H arylation. *J. Am. Chem. Soc.* **146**, 228–239 (2024).
62. Pan, Z. H., Liu, M. L., Zheng, C. Y., Gao, D. Q. & Huang, W. Study of Karstedt's catalyst for hydrosilylation of a wide variety of functionalized alkenes with triethoxysilane and trimethoxysilane. *Chin. J. Chem.* **35**, 1227–1230 (2017).
63. Doll, J. S., Heldner, M. L., Scherr, M., Ballmann, J. & Rosca, D.-A. The atmosphere matters: the effect of "Inert" gas on the catalytic outcomes in cobalt-mediated alkyne and olefin hydroboration. *ACS Catal.* **13**, 8770–8782 (2023).
64. Guo, J., Cheng, Z. Z., Chen, J. H., Chen, X. & Lu, Z. Iron- and cobalt-catalyzed asymmetric hydrofunctionalization of alkenes and alkynes. *Acc. Chem. Res.* **54**, 2701–2716 (2021).
65. Chen, C. H. et al. Iron-catalyzed asymmetric hydrosilylation of vinylcyclopropanes via stereospecific C-C Bond cleavage. *iScience* **23**, 100985 (2020).
66. Cheng, B., Lu, P., Zhang, H. Y., Cheng, X. P. & Lu, Z. Highly enantioselective cobalt-catalyzed hydrosilylation of alkenes. *J. Am. Chem. Soc.* **139**, 9439–9442 (2017).
67. Chen, J. H., Cheng, B., Cao, M. Y. & Lu, Z. Iron-catalyzed asymmetric hydrosilylation of 1,1-disubstituted alkenes. *Angew. Chem. Int. Ed.* **54**, 4661–4664 (2015).

Acknowledgements

The authors thank National Key Research and Development Program of China (2021YFA1500200), National Natural Science Foundation of China (NSFC) (22271249), Zhejiang Provincial Natural Science Foundation of China (LDQ24B020001), the Fundamental Research Funds for the Central Universities (226-2022-00224 and 226-2024-00003), the Center of Chemistry for Frontier Technologies, and Xinjiang Key Laboratory of Organosilicon Functional Molecules and Materials. We thank Tongtong Li for repeating the construction of **3a**, Zhanchen Ye for repeating the construction of **10a**, Lixuan Zheng for the synthesis of **2s**, Zikai Qian for the synthesis of **2r**. We also thank Jiyong Liu for X-ray crystallographic analysis; Luling Wu, Yaqin Liu for NMR analysis; Qiaohong He for ESI-HRMS analysis from Analysis and Test Platform of Department of Chemistry, Zhejiang University.

Author contributions

Conceptualization, Z.L.; Methodology, X.W, J.J.Z., D.Y.W. L.D.; Investigation, X.W., and J.J.Z.; Writing-original draft, Z.L. and X.W.; Writing-review & editing, Z.L., and X.W.; Funding Acquisition, Z.L. and L.D.; Supervision, Z.L. and L.D.

Competing interests

The authors declare no competing interest.

Additional information

Supplementary information The online version contains supplementary material available at https://doi.org/10.1038/s41467-025-59364-3.

Correspondence and requests for materials should be addressed to Zhan Lu.

Peer review information *Nature Communications* thanks Liangbin Huang, and the other, anonymous, reviewer for their contribution to the peer review of this work. A peer review file is available.